POLITECNICO DI TORINO
Repository ISTITUZIONALE

Conceptual design and optimisation of a novel hybrid device for capturing offshore wind and wave energy

Terms of use:

Publisher copyright

(Article begins on next page)

28 April 2024

Conceptual design and optimisation of a novel hybrid device for capturing offshore wind and wave energy

E. Faraggiana[1] · M. Sirigu[1] · A. Ghigo[1] · E. Petracca[1] · G. Mattiazzo[1] · G. Bracco[1]

Abstract

The access to the offshore wind resource in the deep sea requires the development of innovative solutions which reduce the cost of energy. Novel technologies propose the hybrid combination of wind and wave energy to improve the synergy between these technologies sharing costs, such as mooring and electrical connexion. This work proposes a novel hybrid wind and wave energy system integrating a floating offshore wind turbine with three-point absorbers wave energy converters (WECs). The WECs are an integral part of the floating structure and contribute significantly to the hydrostatic and dynamic stability of the system. Their geometry is optimised considering a cylindrical, semi-cylindrical and spherical shape for the Pantelleria case study. The cylindrical shape with the largest radius and the lowest height is the optimal solution in terms of reducing structural costs and maximising the performance of the WECs. The in-house hydrostatic stability tool and the time domain model MOST are used to optimise the WECs, with a combined meta-heuristic genetic algorithm with the Kriging surrogate model and a local Nelder–Mead optimization in the final simulations. The power of the WECs is estimated with both linear and variable motor flow hydraulic PTOs to obtain a more realistic electrical power generation. Generally, the hybrid device proved to be more competitive than the floating wind turbine alone, with a LCOE reduction up to 11%. Performance of the hybrid device can be further improved when more energetic sites are considered, as the energy generated by the WECs is higher.

1 Introduction

Offshore renewable energy technologies have enormous potential as they are still at an early development stage. The European Green Deal supports the energy transition towards de-carbonisation of the supply chain and includes a strategy for offshore renewable energy technologies (Hainsch et al. 2020). The main target is to achieve 300 GW and 40 GW from offshore wind and ocean energy respectively in Europe by 2050. A multi-purpose approach for an offshore renewable energy technology is preferred as it is possible to combine multiple marine activities in a single area. There are different examples of EU-funded projects which have studied multi-purpose platforms including combined wind–wave energy and the economic and environmental benefits of these projects (Fraunhofer-Gesellschaft 2011; UL Solutions Spain 2014; Acciona 2015; PLOCAN 2015; WWF France 2023).

A project combining wind and wave energy for energy extraction offers several synergies, such as more consistent power output, shared grid connexion, foundations, logistics and maintenance costs (Pérez-Collazo et al. 2015). The hybrid system is classified into bottom-fixed and floating systems. The first type is limited to shallow water depths, whilst the second aims to harness a greater wind resource in deep waters. The bottom-fixed offshore wind technology

✉ E. Faraggiana
  emilio.faraggiana@polito.it

  M. Sirigu
  massimo.sirigu@polito.it

  A. Ghigo
  alberto.ghigo@polito.it

  E. Petracca
  ermando.petracca@polito.it

  G. Mattiazzo
  giuliana.mattiazzo@polito.it

  G. Bracco
  giovanni.bracco@polito.it

[1] Department of Mechanical and Aerospace Engineering, Polytechnic University of Turin, 10129 Turin, Italy

has reached a more advanced development stage compared to floating offshore wind technology, as it is more similar to the established onshore wind technology (Lee and Zhao 2021). However, floating wind has a larger potential than bottom-fixed, as an estimated 80% of the world's offshore wind potential lies in water depths greater than 60 m (Lee and Zhao 2021), where floating wind power technology is more suitable. Floating hybrid devices can be combined with a large variety of types of WECs, generally belonging to the family of point absorbers, oscillating wave surge converters (or flaps) and oscillating water columns (OWCs) (Karimirad 2014; Pérez-Collazo et al. 2015; McTiernan and Sharman 2020). Multiple point absorbers and flaps are suitable for a semi-submersible floating offshore wind platform as they cover a large near-surface area from which the WECs can be installed. The main benefit of using flaps is that they can be completely removed from the water during large storms, which extends their service life. OWCs require a chamber to operate and have been coupled with the columns of Semi-submersible platforms, such as the WindFloat and DeepCwind (Weinsten and Ho 2011; Zhang et al. 2022).

Recently, hybrid solutions for offshore wind and wave energy have been developed to obtain a more competitive device compared to offshore wind alone. Wave Treader (Green Ocean Energy 2023) and WEGA (Sea For Life 2022) are two examples of hybrid solutions that combine a bottom-fixed wind turbine with a point absorber. The main advantage of these hybrid solutions is that the Wave Energy Converters (WECs) can be easily integrated without any major change to the bottom-fixed technology. W2Power, developed by Pelagic Power AS, is one of the most successful examples of a floating hybrid wind device, combining two wind turbines in the front corners and multiple heave point absorber WECs on the same semi-submersible platform (Hanssen et al. 2015). Another well-known example of a floating hybrid platform is the Poseidon platform developed by Floating Power Plant Ltd which has also been funded by Horizon 2020 (Floating Power Plant Ltd 2017).

There are several floating hybrid wind platforms that have been investigated in different research projects. The WindWaveFloat was studied in Weinsten and Ho (2011) considering four configurations of the WindFloat (Roddier et al. 2010) and different types of Wave Energy Converters (WECs) including OWCs, point absorbers and flaps. It is found that the WECs have a minor impact on the platform motion and wind energy production. Another possible hybrid solution is the Hywind concept in combination with a Spar Torus Concept (STC) WEC (Muliawan et al. 2013; Wan et al. 2016). The power from the WEC is generated by the relative heave motion between the spar and the torus. The estimated total power production from the combined system demonstrated to be about 10–15% higher than that of the spar alone

(Muliawan et al. 2013). In Wang et al. (2020), the preliminary sizing of a semi-submersible floating wind platform in combination with a Heave Point absorber inspired by the STC concept was investigated. The hybrid combination of Hywind with the STC concept was also proposed in Li et al. (2018) by adding tidal turbines that harvest energy from the ocean current. The total power production increased by 22–45% depending on environmental conditions. A semi-submersible Flap Combination (SFC) comprising a semi-submersible platform with 3 WECs of the flap type was analysed in Luan et al. (2014), Michailides et al. (2016). The numerical model of the SFC was validated with experimental results and it was found that the WECs have no effect on the mooring line tension, nacelle acceleration and bending moment at the tower base (Michailides et al. 2016). The combination of the Fincantieri Sea Flower Floater and the ISWEC gyroscopic device was shown to improve the stability of the floater and reduce hull pitch motions up to 37% (Fenu et al. 2020). A novel concept combining the Nautilus platform and four point absorbers was investigated in Petracca et al. (2022). The hybrid concept showed a 10% reduction in the Levelised Cost of Energy (LCOE) and improved hydrodynamic stability compared to a floating wind turbine. A feasibility study integrating the Hywind wind turbine platform with WEC's WaveStar type (Marquis et al. 2012) is assessed in Karimirad and Koushan (2017). The study successfully concludes that the WEC has a negligible impact on the wind turbine performance whilst improving the total power generated by the turbine by more than 6%. The hybrid combination of the DeepCWind semi-submersible wind turbine and a various numbers of the WaveStar WECs is investigated in Ghafari et al. (2021) and it is concluded that a larger number of WECs leads to a more stable platform, a lower sensitivity to the wave direction and a larger power to Response Amplitude Operator (RAO) ratio.

In the present study, a hybrid combination of a semi-submersible platform and three WaveStar WECs is investigated. The aim is to tackle the problem of reducing LCOE of a semi-submersible floating wind turbine converting structural floating bodies into WECs. The numerical modelling methodology is the same as in previous publications (Faraggiana et al. 2022b; Sirigu et al. 2022b) and is based on linear potential flow theory, blade element momentum theory and time domain simulations. The hybrid device is optimised for some geometry design parameters to minimise the structural cost and maximise the power of the WECs. The WECs are investigated for three different geometries: semi-cylindrical, cylindrical, and spherical shapes. The optimal design solution is finally modelled to include a more realistic hydraulic Power-Take-Off (PTO) system and compared in terms of performance with a floating wind turbine system alone.

This paper first describes the design of the hybrid system in Sect. 2.1. The numerical model and the optimisation

Table 1 Design properties of the floating wind turbine

Mooring system	Number of mooring lines (n_M)	3
	Anchor depth, radius from centerline (m)	320, 854.67
	Fairlead depth, radius from centerline (m)	20, 6
	Unstretched mooring line length, diameter (m)	902.2, 0.09
	Mooring line density (kg/m)	77.7
	Total vertical pre-load (MN)	2.247
Tower	Base, top elevations (m)	10, 87.6
	Base, top diameters (m)	6.5, 3.87
	Mass (kg)	249,718
Rotor-nacelle	Rotor diameter (m)	126
	Hub height (m)	90
	Mass (kg)	350,000
Floating platform	Central cylinder and arm material density $\left(\frac{kg}{m^3}\right)$	Steel, 8500
	WEC material density $\left(\frac{kg}{m^3}\right)$	Concrete, 2400
	Ballast material density $\left(\frac{kg}{m^3}\right)$	Magnetite, 5200
	Steel shell thickness (m)	0.07
	α_0 (deg)	95
	R_{arm} (m)	1
	H_A (m)	3
	H_B (m)	3

approach are described in Sects. 2.2 and 2.3, respectively. Details of the techno-economic analysis comparing the hybrid system and the floating wind turbine system alone are given in Sect. 2.4. The optimisation results are given in Sects. 3.1 and 3.2, whilst the results of the techno-economic analysis are given in Sect. 3.3. Finally, Sects. 4 and 5 present the discussion and conclusion.

2 Materials and methods

2.1 Design of the hybrid system

The hybrid system is composed of the NREL 5 MW wind turbine (Jonkman et al. 2009) and by three WaveStar WECs. The wind turbine is a three-bladed, horizontal-axis wind turbine mounted above the floating platform. The main properties of the floating wind turbine are described in Table 1.

The floating platform consists of a central cylinder with some ballast in the lower part of the cylinder. The central cylinder has reduced dimensions (height) to be installed in

shallow water (60 m) and to allow installation in the shipyard. The static and dynamic stability is mainly achieved by the WECs, which are connected to the central cylinder via arms. The WECs generate electrical energy through the rotation of the WEC arms around the hinges arranged around the central cylinder. Each WEC arm is connected to a hydraulic PTO which converts the arms' mechanical rotational energy into hydraulic and electrical energy. The hybrid device includes a safety lock between the WEC arms and the central cylinder fixing their relative position in the event of PTO failures and extreme environmental conditions to ensure sufficient structural integrity and floating stability. This safety system saves costs in the design of WECs' PTO as the highest peaks of PTOs' force and power will be avoided by switching the device to a survival mode and activating the lock.

The design optimisation of the WECs considered three different geometries of the WECs, which result in different response to waves and different structural costs. A conceptual schematic of the device for the cylindrical type of WEC is shown in Fig. 1, whilst the three different geometries, which include spherical, cylindrical and semi-cylindrical shapes, are shown in Fig. 2. The layout of the WECs is given in Fig. 3 and is similar to the different WEC geometries, whilst the wave and wind directions are the same and represented by the x-axis. The optimisation design parameters are shown in Figs. 1, 2, whilst a description of the studied area for each design parameter can be found in Table 2. The optimisation design parameters include both the geometry and PTO parameters.

The main material of the floating platform is steel and a constant thickness of 7 cm is considered to estimate the total steel weight, similarly to the Innwind deliverable (Danmarks Tekniske Universitet 2014). Concrete was chosen as the material for the WECs whilst the concrete thickness is calculated to maintain hydrostatic torque balance on each arm around the hinge. In this way, there is no need to pre-load each arm to maintain the static position of the WECs, which results in a cost saving for the hydraulic PTO, as no auxiliary tank would be required. The thickness of the WECs is calculated automatically and depends on the geometry of the WEC. The mass of the float is calculated imposing the hydrostatic balance on the WEC hinge:

$$F_{NBarm} \cdot x_{arm} + F_{NBfloat} \cdot x_{float}$$
$$= -M_{arm}g \cdot x_{arm} + (B_{float} - M_{float}g) \cdot x_{float} = 0, \quad (1)$$

where F_{NBarm} and $F_{NBfloat}$ are the net buoyancy of the WEC arm and the WEC float, M_{arm} and M_{float} are the masses of the arm and the float, B_{float} is the buoyancy of the float and x_{arm} and x_{float} are the distance between the hinge and the hydrostatic and gravity loads on the arm and on the float, respectively.
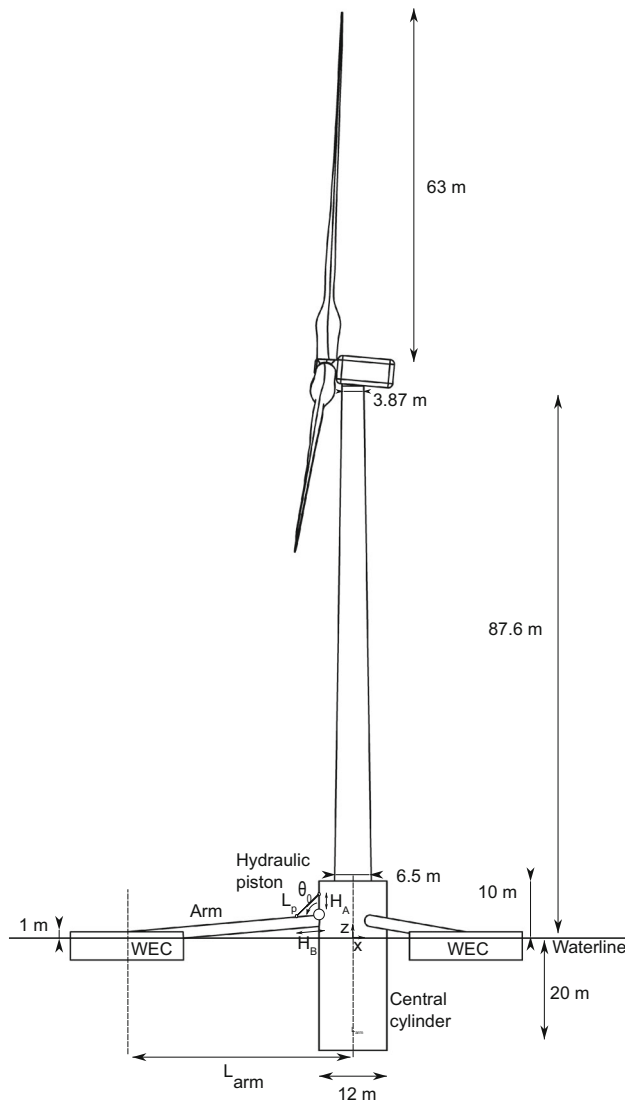
Fig. 1 Design scheme of the floater

The thickness of the WECs is obtained solving the following equations respectively for the spherical, cylindrical and semi-cylindrical shapes:

$$t^3 - 3R_{\text{wec}}t^2 + 3R_{\text{wec}}^2 t - \frac{M_{\text{float}}}{\frac{4}{3}\pi\rho_{\text{concrete}}} = 0, \tag{2}$$

$$2t^3 + t^2\left(-H_{\text{wec}} - 4R_{\text{wec}}\right)$$
$$+ t\left(2R_{\text{wec}}^2 + 2R_{\text{wec}}H_{\text{wec}}\right) - \frac{M_{\text{float}}}{\pi\rho_{\text{concrete}}} = 0, \tag{3}$$

$$t^3(4+\pi) + t^2\left(-4 - 4R_{\text{wec}} - 2H_{\text{wec}} - \frac{\pi}{2}H_{\text{wec}} - 2\pi R_{\text{wec}}\right)$$
$$+ t\left(4R_{\text{wec}} + 2H_{\text{wec}} + 2R_{\text{wec}}H_{\text{wec}} + R_{\text{wec}}^2\pi + R_{\text{wec}}H_{\text{wec}}\pi\right)$$
$$- \frac{M_{\text{float}}}{\rho_{\text{concrete}}} = 0, \tag{4}$$

where t is the thickness, R_{wec} is the WEC radius, H_{wec} is the WEC height.

Finally, the ballast is assumed to be magnetite due to the high material density and low price.
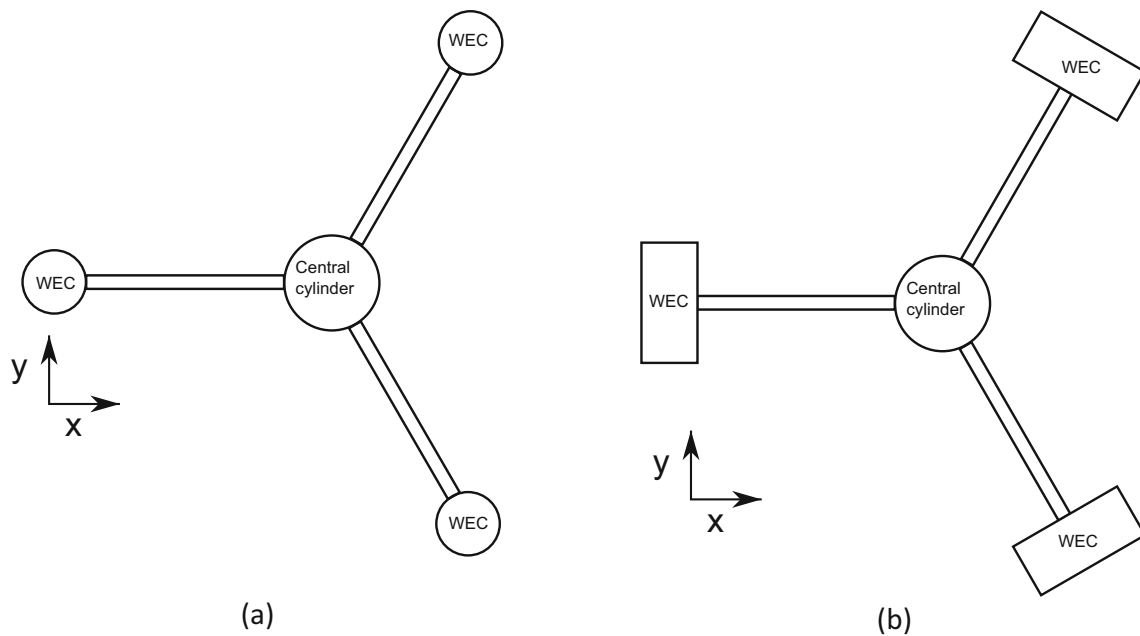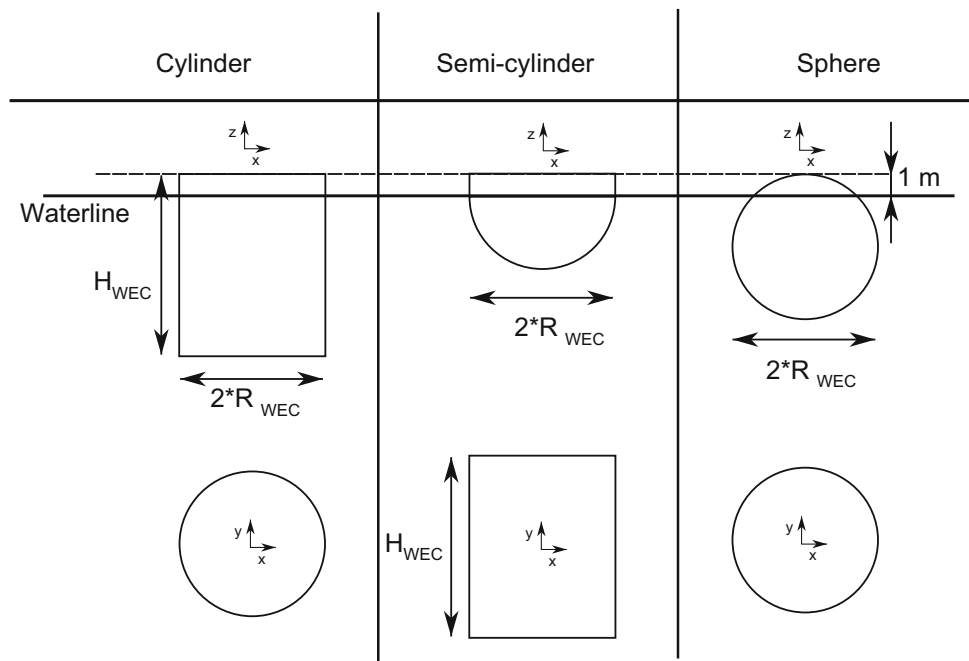
2.2 Numerical model

The simulation of the hybrid device is made in a MATLAB environment that connects different software which are open-source or in-house codes, similar to what is described in Faraggiana et al. (2022b) (See Fig. 4). The open-source platform SALOME was used to create the CAD model and the mesh (EDF Energy 2023). In particular, this calculation was automated using the text user interface (TUI) of SALOME to be suitable for an optimisation algorithm. Salome is also used to obtain further properties of the platform, such as the inertia moments, the Center of Gravity (COG) and the displaced volume of each body (WECs and central tower). The design configuration is then first assessed using the in-house Hydrostatics and Stability tool, computing stability properties of the floating device, such as the static pitch angle and metacentric height. The hydrodynamic coefficients are calculated using Nemoh based on the meshes provided by Salome and the computed COG. Finally, the dynamic simulation of the floating platform is computed using the in-house code MOST (Faraggiana et al. 2022b; Sirigu et al. 2022b). The dynamic simulation is performed to evaluate the dynamic stability of the platform and to compute the power generated by the WECs.

2.2.1 Hydrostatic stability tool

The geometry configuration generated in Salome-Meca is assessed using the stability tool implemented in MATLAB. This tool has been previously verified with the commercial code Orca3D (Faraggiana et al. 2022b; Petracca et al. 2022). The hydrostatic stability is checked for the free-floating condition of the hybrid device and so without the mooring. The stability tool calculates the static pitch angle, the metacentric height and the righting moment curve and are compared with DNV recommended values (DNV-GL 2018). The DNV standard recommends a metacentric height more than 1 whilst the area under the righting moment curve until the second intercept should be equal or greater than 130% the area under the wind heeling moment. A maximum static pitch angle of 15° is also considered in the optimisation.

The static pitch angle is determined by the first interception between the righting moment and the wind heeling curves. The heeling righting moment is calculated for each heeling angle using the "fminsearch" MATLAB function to obtain the same displaced volume and a trim righting torque equal to 0. So, each heeling angle is associated to a sinkage and a trim value. Furthermore, the position of the COG is

Fig. 2 Different geometries of the WEC

Cylinder Semi-cylinder Sphere

Waterline

H_{WEC}

$2*R_{WEC}$

$2*R_{WEC}$

$2*R_{WEC}$

1 m

H_{WEC}

WEC

WEC

Central cylinder

WEC

WEC

WEC

Central cylinder

WEC

WEC

(a)

(b)

Fig. 3 Layout of the WECs for the cylindrical and spherical shape (**a**) and the semi-cylindrical shape (**b**). Wave and wind directions are shown by the *x*-axis

updated for the new position of the platform. The righting moment ($\overrightarrow{M}_R$) is computed from the hydrostatic pressures from the mesh given from Salome-Meca updated for the heeling, trim and sinkage values:

$$\overrightarrow{M}_R = \sum_{ip=1}^{iN} \rho_w g z_i \overrightarrow{A}_{ip} \times \overrightarrow{D}_{ipG}, \qquad (5)$$

where ρ_w is the water density, z_i and $\overrightarrow{A}_{ip}$ are the depth and the area vector of each panel whilst $\overrightarrow{D}_{ipG}$ is the vector connecting the centre of each panel and the COG.

The wind heeling moment is estimated from the heeling moments due to the tower and the rotor:

Table 2 Optimisation design parameters

Sphere	R_{wec} (m)	[2 15]
	L_{arm} (m)	[25 80]
Cylinder	R_{wec} (m)	[2 15]
	H_{wec} (m)	[2 21]
	L_{arm} (m)	[25 80]
Semi-cylinder	R_{wec} (m)	[2 15]
	H_{wec} (m)	[5 50]
	L_{arm} (m)	[25 80]
PTO design parameters	k_{PTO} (MNm/rad)	[1 3000]
	c_{PTO} (MNms/rad)	[1 3000]

$$M_{\text{w}} = M_{\text{Wt}} + M_{\text{Wr}}$$
$$= \frac{1}{2}\rho_{\text{air}}\left(\int_{h\text{min}}^{h\text{max}} C_{Dt}v(h)^2 D(h)h\,\mathrm{d}h + c_{T\text{max}}V_{\text{r}}^2 A_{\text{r}}h_{\text{r}}\right)\cos(\alpha_{\text{h}}),$$
$$(6)$$

where ρ_{air} is the air density, C_{Dt} is the drag coefficient of the tower, $v(h)$ is wind speed that follows the logarithmic wind speed profile, $D(h)$ is the diameter of the tower for each height, h_{min} and h_{max} are the distance between the centre of buoyancy (COB) and the bottom and top position of the tower, $c_{T\text{max}}$ and V_{r} are the maximum thrust coefficient and the wind speed associated, A_{r} is the swept area, h_{r} is the rotor height relative to the COB and α_{h} is the heeling angle. The COB has been chosen for the calculation of the wind heeling arm as the DNV standard suggests the centre of lateral resistance of the underwater body.

The metacentric height (GM) can be calculated for small heeling angles (α_{h}) as

$$\text{GM} = \frac{M_{\text{R}}}{\rho_{\text{w}}g V_{\text{d}}\sin(\alpha_{\text{h}})}, \qquad (7)$$

where V_{d} is the displaced volume.

2.2.2 Time-domain model

The time domain simulation is performed in MOST to assess the dynamic stability. Dynamic stability is assessed by computing the maximum dynamic pitch angle (less than 15°)

and the rms of the nacelle acceleration (less than 2 m/s^2) which are used as constraints in the optimisation. MOST has been verified in previous work with the well-known software Fast (Sirigu et al. 2022a, b). MOST is an aero-hydro-servo model which can simulate floating offshore wind turbines and hybrid systems in 6 degrees of freedom. The simulation time is 1300 s with a timestep of 0.05 s and MATLAB ode4 using the Runge–Kutta method. The loads applied on the floating offshore wind turbine are obtained in a similar way as described in a previous paper (Faraggiana et al. 2022b). The hydrodynamic time-dependent loads are estimated from the hydrodynamic frequency coefficients calculated for the four hydrodynamic bodies (central cylinder and the three WECs) using the open-source Nemoh (Babarit and Gérard 2015). Nemoh is based on linear potential flow theory, which assumes an inviscid, irrotational and incompressible flow. The radiation and excitation forces ($F_{\text{rad}}(t)$, $F_{\text{exc}}(t)$) for each hydrodynamic body (WECs and central cylinder) have been calculated respectively as

$$F_{\text{rad}}(t) = -A_{\infty}\ddot{X} - \int_0^t K_{\text{r}}(t-\tau)\dot{X}(\tau)\mathrm{d}\tau, \qquad (8)$$

and

$$F_{\text{exc}}(t) = \text{Re}\left(\sum_{j=1}^{N} F_{\text{exc}}(\omega_j, \theta)\mathrm{e}^{i(\omega_j t + \phi_j)}\sqrt{2S(\omega_j)\mathrm{d}\omega_j}\right), \qquad (9)$$

where A_{∞} is the infinite added mass matrix, K_{r} is the radiation impulse response function, ω and Φ are the wave and phase frequencies, $S(\omega)$ is the wave spectrum and $\dot{X}$ and $\ddot{X}$ are the velocity and acceleration vectors. The radiation force accounts for the hydrodynamic interaction, as the infinite added mass and the radiation impulse response function include the hydrodynamic coupling between the degrees of freedom of a certain body and the degrees of freedom of all bodies.

The viscous force (F_{v}) is also included in time domain using a quadratic relationship with the body velocity:

$$F_{\text{v}} = -0.5c_{\text{d}}\rho_{\text{w}}A_{\text{d}}\dot{X}|\dot{X}|, \qquad (10)$$

Fig. 4 Overall simulation scheme
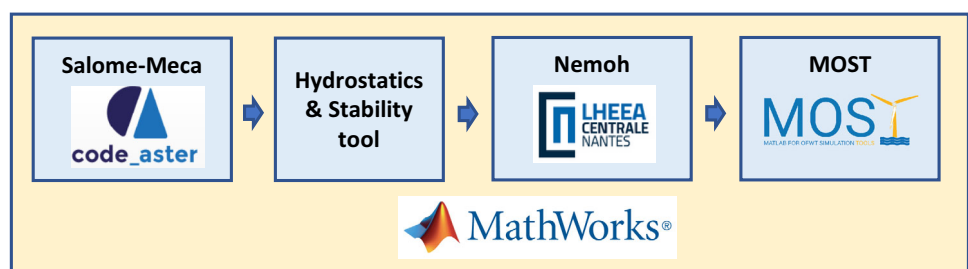
Table 3 Drag coefficients used in the simulation

	Surge	Sway	Heave	Roll	Pitch	Yaw
Cylinder	0.7	0.7	0.9	0.7	0.7	0.01
Semi-cylinder	0.8	0.9	0.8	0.8	0.01	0.8
Sphere	0.2	0.2	0.2	0.01	0.01	0.01

where c_d is the drag coefficient and A_d is the characteristic area. The selection of the drag coefficient is assumed from literature (Yunus 2010) and it is shown in Table 3.

The aerodynamic loads and the mooring loads are computed using look-up tables in a similar way as described in Faraggiana et al. (2022b) to reduce the simulation time. The mooring is modelled using a quasi-static approach which computes the catenary equation for each single line (Masciola 2018). A look-up table relating the total mooring load to the translational and rotational motion of the platform is created to save computational time during the optimisation.

The aerodynamic loads are calculated using Blade Element Momentum Theory (BEMT) with Prandtl's Tip Loss and Glauert corrections. Aerodynamic torque and thrust loads are discretised as a function of blade pitch, rotor speed and wind speed similar to Faraggiana et al. (2022b). To maximise the generated power, variable speed and variable pitch control are used. A look-up table is used to relate the generator torque and rotor speed, whilst above the rated speed, a proportional-integral (PI) control of the generator speed error is used.

Finally, a more accurate time domain simulation of the hybrid device is performed to verify the extreme environmental conditions described in Sect. 2.2.4. Nonlinear buoyancy and Froude–Krylov are computed in WEC-Sim accounting for the instantaneous sea surface elevation and body position. Mooring is simulated using Moordyn, a lumped-mass dynamic mooring model, more accurate than the quasi-static previous approach.

2.2.3 PTO of the WECs

In this work, two different types of PTO of the WECs were used. In the design optimisation of the float, a linearised PTO was preferred because this study considers the conceptual design of the device, and the hydraulic PTO is not yet defined in detail. With a linearised PTO, the torque on each arm is calculated as follows:

$$T = c_{PTO}\dot{\theta} + k_{PTO}\theta \tag{11}$$

However, for a more accurate estimation of the energy generated by the device, a preliminary choice of hydraulic PTO is made similar to Amini et al. (2022). In particular, the hydraulic PTO considers a double-acting hydraulic piston

pump that converts the kinetic energy of the WECs into a bidirectional fluid flow. The piston is directly coupled to the WEC arms and its position on the central cylinder and each arm is indicated by H_A and H_B as shown in Fig. 1. The PTO force is opposite to the piston velocity and is calculated as follows (So et al. 2015; Quartier 2018):

$$F_{PTO} = (-\text{sign}(v_p))(P_{HPA} - P_{LPA}) \cdot A_p = (-\text{sign}(v_p))\Delta P \cdot A_p, \tag{12}$$

where P_{HPA} and P_{LPA} are the high and low pressures of the accumulator whilst A_p is the piston area.

The piston velocity is calculated from the rotational angle of the WEC arm joint, which is modelled as a "rotational PTO" block of the WEC-Sim library. The instantaneous piston length (L_p) is calculated from the law of cosines considering H_A, H_B and θ. The piston velocity is then obtained deriving the formula of the piston length expressed as

$$V_p = \frac{H_A H_B \cdot \dot{\theta} \cdot \sin(\theta)}{\sqrt{H_A^2 + H_B^2 - 2H_A H_B cos\theta}}. \tag{13}$$

The torque on the WEC arm joint is calculated from the PTO force and the torque arm (r_p) as

$$T_{PTO} = r_p \cdot F_{PTO} = \frac{\sin(\theta)H_A H_B}{L_p} \cdot F_{PTO}, \tag{14}$$

where r_p is calculated considering the law of sines.

The absorber power is obtained as

$$P_{abs} = F_{PTO} \cdot V_p. \tag{15}$$

Rectifying valves are then used to convert the bidirectional fluid flow into a unidirectional flow. The fluid is pumped to a high-pressure accumulator where the hydraulic energy is stored. The fluid power is then converted into mechanical energy using a variable displacement hydraulic motor and then into electrical energy using a generator connected to the same shaft. The generator is a typical industrial asynchronous generator and is modelled as a simple rotational inertia system and a look-up table for calculating the efficiency of the generator as a function of speed and torque.

The incoming flow to the high-pressure accumulator (HPA) is the sum of the piston and the motor flows and can

be calculated as (Quartier 2018)

$$Q_{HPA} = Q_{piston} + Q_{motor} = v_p \cdot A_p + \omega_m \cdot \alpha D, \qquad (16)$$

where ω_m is the angular velocity and αD is the hydraulic motor volume.

The volume of fluid that flow into the HPA (V_{in}) can be calculated by the time integral of Q_{HPA}. The instantaneous pressure inside the HPA can be determined by considering an isentropic process and is computed as (So et al. 2015)

$$P_{HPA} = \frac{P_{pre\text{-}charge}}{\left(1 - \frac{V_{in}}{V_{HPA}}\right)^{1.4}}, \qquad (17)$$

where $P_{pre\text{-}charge}$ is the pre-charge pressure inside the accumulator.

The pressure of the low-pressure accumulator (LPA) is calculated in a similar way considering the fluid flow inside the LPA with the opposite sign compared to the flow inside HPA.

The angular velocity of the hydraulic motor is calculated as (Quartier 2018)

$$\dot{\omega}_m = \frac{\Delta P \cdot \alpha D - T_g - T_f}{I_{mg}}, \qquad (18)$$

where T_g and T_f are the generator and the frictional torques, I_{mg} is the total moment of inertia of the motor/generator. T_f is assumed 5% of T_g whilst I_{mg} is assumed 20 kgm^2.

The generator torque is calculated as (Amini et al. 2022)

$$T_g = \Delta P \cdot \alpha D \frac{\omega_m}{\omega_{desired}} \cdot \frac{1}{1.05}, \qquad (19)$$

where $\omega_{desired}$ is 150 rad/s and 1.05 accounts for the mechanical efficiency.

The fluid motor is modelled dependent on the pressure difference between the accumulators, and it is expressed as

$$\begin{cases} \Delta P < 4\text{MPa} \rightarrow \alpha D = 2e^{-5} \\ 4\text{MPa} < \Delta P < 15\text{MPa} \rightarrow \alpha D = 2.67e^{-11}\Delta P - 8.52e^{-5} \\ \Delta P > 15\text{MPa} \rightarrow \alpha D = 3.153e^{-4} \end{cases}$$
$$(20)$$

The power fluctuation ratio (R_f) is defined as

$$R_f = \frac{P_{high} - P_{low}}{P_{wecr}}, \qquad (21)$$

where P_{low}, P_{high} and P_{wecr} are the minimum, maximum and rated power of each WEC.

2.2.4 Environmental conditions

The environmental conditions were determined for an offshore site near Pantelleria (LAT = 37.01°, LONG = 12.02°), which is suitable for the use of marine energy. The environmental conditions considered for the simulations for Pantelleria are significant height (H_s), energy period (T_e) and wind speed (V_0), whilst wind and wave direction are assumed to be coincident and constant during the simulation. We have also not considered the influence of the marine current, as it is assumed to have a minor influence in the Mediterranean Sea. The wave elevation is simulated with a Jonswap spectrum in MOST, whilst wind is modelled with the power law wind speed profile with a power coefficient of 0.14 and the IEC Kaimal turbulence model in NREL Turbsim software (Jonkman and Buhl Jr 2006). A two-dimensional grid of 280 m × 280 m with a discretization of 17 × 17 points is used to obtain the wind turbulence values for each timestep of the time domain simulation. The wind speed values are then interpolated and averaged for four different points along the blade length. The relative wind speed on each blade, which is used to calculate the aerodynamic loads, is corrected to account for the normal projection onto the blade and the additional speed of the nacelle.

Hourly data of H_s, T_e and V_0 have been collected from the ERA5 database (ECMWF 2022) from 2010 to 2019 and the coordinates provided. A finer and a coarser discretisation of all collected triplets are shown in Fig. 5. The finer discretization (Fig. 5a) considers a discretization step of 0.25 for H_s, T_e and V_0 whilst the coarser discretization (Fig. 5b) considers a discretization step of 1 m for H_s, 3 s for T_e and 4 m/s for V_0. The triplets from the coarser discretization (61) are then selected based on occurrence, wind and wave energy potential (> 99.6%). The wind and the wave energy potentials of each triplet are calculated as

$$P_{Wind} = \frac{1}{2}\rho A_r V_0^3, \qquad (22)$$

and

$$P_{Wave} = 0.49 H_s^2 T_e, \qquad (23)$$

The final triplets (47) (Fig. 5b) are used to calculate the energy production of the device. A representative triplet with the largest thrust, severe wave conditions and the most occurrent energy period (H_s = 6 m, T_e = 7 s and V_0 = 11 m/s) is chosen to verify the dynamic stability of the platform and to optimise the geometry of the WECs similar to Faraggiana et al. (2022b, c).

Finally, extreme environmental conditions have been used to verify the survivability of the device. The extreme conditions are selected from the environmental contour shown in

Fig. 5 Environmental conditions for a fine (**a**) and a coarse (**b**) discretization of the significant height, energy period and wind speed
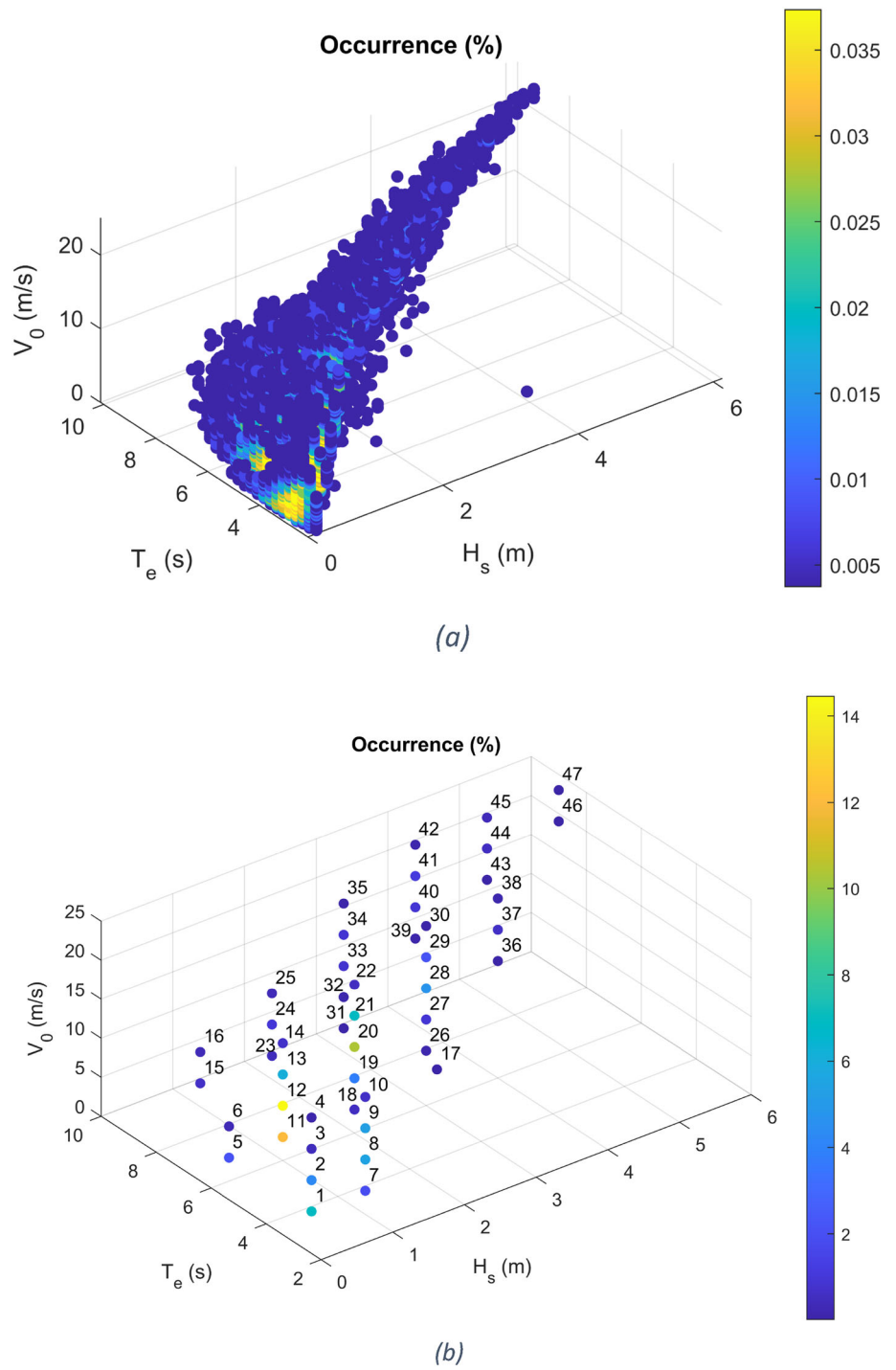

(a)

(b)

Fig. 6 and represent the largest H_s ($H_s = 7.33$ m, $T_e = 9.89$ s and $V_0 = 26.14$ m/s) and the largest wind speed ($H_s = 7.11$ m, $T_e = 9.78$ s and $V_0 = 26.69$ m/s). The environmental contour of Pantelleria has been obtained using the IFORM approach described in DNV (2010) with a return period of 50 years.

2.3 Design optimisation

The design optimisation first aims to obtain an optimal design of the WEC geometry using a preliminary linear PTO loading model. This PTO model provides an optimistic estimate of the generated power that could approximate the PTO loading of discrete displacement hydraulic cylinders (Henderson

Environmental Contour
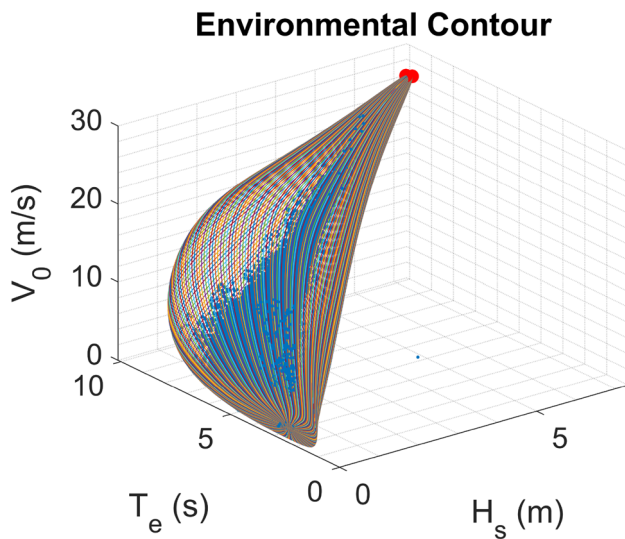
Fig. 6 Environmental contour of Pantelleria. Selected extreme environmental conditions are shown in red (colour figure online)

Table 4 Main optimisation parameters

	2 design parameters	3 design parameters
Population	15	15
Generations	3	10
Crossover probability	0.9	0.9
Mutation probability	0.1	0.1
Elitism factor	0.2	0.2
fminsearch simulations	20	30

2006). Subsequently, the design parameters of a variable displacement hydraulic motor are optimised for the optimal WEC geometry to obtain a more realistic PTO model that takes into account the hydraulic components (accumulators, pistons, motor, and generator).

The optimisation of the WEC geometry considers three different geometries, as explained earlier, and 2–3 design parameters for each geometry (see Table 2). The optimisation algorithm of this study has been used in previous work (Faraggiana et al. 2020, 2022a; b). The algorithm is a free gradient and global optimisation algorithm which combines the genetic algorithm and the Kriging surrogate model. Then, the optimum is refined with MATLAB's optimisation function "fminsearch", which is a local optimisation algorithm but has a faster convergence rate. The main optimisation parameters are listed in Table 4. The optimisation parameters are different when the number of parameters is two (spherical WECs) or three (cylindrical and semi-cylindrical shapes). The design optimisation also includes the PTO coefficients (k_{PTO} and c_{PTO}) which are optimised for each geometry configuration.

The optimisation of the two parameters first involves 10 evaluations with the Latin Hypercube design and then another 10 iterations using the "fminsearch" function. The optimisation approach is shown in Fig. 7.

The objective function used to optimise the geometry of the floats is obtained from the ratio of the material cost of the platform (C_p) and the energy generated by the WECs (E_{wecs}):

$$
\begin{aligned}
f_{cost1} &= \frac{C_p}{E_{wecs}} \\
&= \frac{m_{steel} \cdot c_{steel} + m_{concrete} \cdot c_{concrete} + m_{ballast} \cdot c_{ballast}}{\frac{9}{36} P_{wecs} \cdot 8760}
\end{aligned}
\tag{24}
$$

where C_p is determined by multiplying the mass and specific cost of steel ($c_{steel} = 3 \,€/kg$), concrete ($c_{concrete} = 0.25 \,€/kg$) and ballast ($c_{ballast} = 0.12 \,€/kg$), and E_{wecs} is obtained by multiplying by the number of hours in the year and a proportional ratio to give a more sensible value of the energy generated, from the power generated by the WECs (P_{wecs}). In fact, a more representative value for calculating the amount of energy produced would be 3 m instead of the chosen 6 m, as most of the wave energy potential for Pantelleria is in this range (Sirigu et al. 2020). In particular, the proportional ratio (9/36) is obtained considering the quadratic relationship of the wave energy potential with H_s (Pecher and Kofoed 2017).

Then a more realistic hydraulic PTO has been optimised for the optimal geometry configuration found. Hydraulic PTO parameters considered in the optimisation are the piston area, the HPA volume and the LPA pre-charge pressure whilst their optimisation range is described in Table 5. The LPA volume is kept constant at 0.5 m³ as it affects the results less compared to the other design parameters, as described in Amini et al. (2022).

The objective function is updated to also account the cost of the hydraulic PTO (C_{PTO}):

$$
f_{cost2} = \frac{C_p + C_{PTO}}{E_{wecs}},
\tag{25}
$$

The prototypal estimation of the PTO cost is obtained from Bonfanti (2021) as

$$
C_{PTO} = C_{piston} + C_{acc} + C_{man} + C_{aux} + C_{motor},
\tag{26}
$$

where C_{piston}, C_{acc}, C_{man}, C_{aux} and C_{motor} are the costs of the piston, the accumulator, the manifolds, the auxiliary system, and the motor. C_{man} has been assumed as a fixed term (15 k€).

The piston cost is obtained as (Bonfanti 2021)

$$
C_{piston} = c_{ap} \cdot A_p,
\tag{27}
$$

Fig. 7 Optimisation diagram of the design configurations (three design parameters)
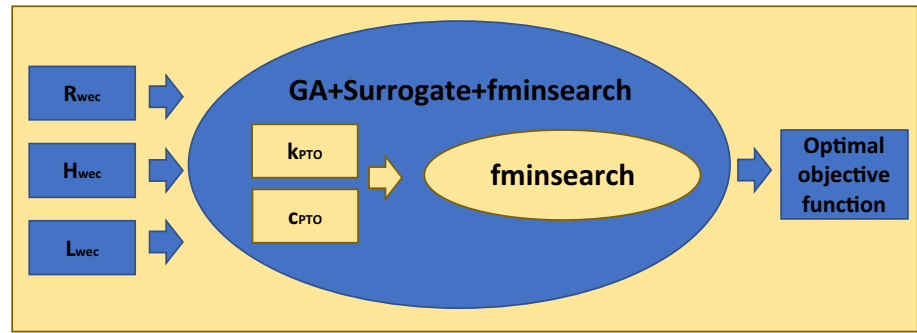

Table 5 Optimisation range of hydraulic PTO design parameters

Piston area (m^2)	[0.045 0.3]
HPA volume (m^3)	[0.5 10]
LPA Pre-charge pressure (MPa)	[3.5 9.6]

where c_{ap} is the specific cost of the piston due to the piston area (1.4076 M€/m^2).

The accumulator cost (C_{acc}) is obtained as (Bonfanti 2021)

$$C_{acc} = (n_{HPA} + n_{LPA}) \cdot C_{junc} + (V_{HPA} + V_{LPA}) \cdot c_v \qquad (28)$$

where n_{HPA} and n_{LPA} are the number of high- and low-pressure accumulators, C_{junc} (250€) is the cost of junctions and tubes connecting each accumulator to the manifold, V_{HPA} and V_{LPA} are the volumes of the high and low-pressure accumulators and c_v (22 €/l) is the specific cost of the accumulators. The number of high- and low-pressure accumulators is obtained assuming a maximum single accumulator capacity of 600 m^3.

The auxiliary cost (C_{aux}) and the motor cost (C_{motor}) are obtained respectively as (Bonfanti 2021)

$$C_{aux} = C_{valves} + C_{oil} = C_{valves} + V_{oil} \cdot c_{oil}, \qquad (29)$$

and

$$C_{motor} = c_{motor} \cdot P_{wecr}, \qquad (30)$$

where C_{valves} (5 k€) is the valves cost, V_{oil} and c_{oil} (4.5 €/l) are the volume and the specific cost of the oil, c_{motor} (1667 €/kW) and P_{wecr} are the specific cost of the motor and the rated power of each WEC. V_{oil} is obtained as 1.3 times the low-pressure accumulator volume.

A second estimation of the overall hydraulic PTO cost is assumed from Chozas and Kofoed (2014) to be 340 €/kW for industrial/series production.

Finally, the energy produced from the hybrid device is compared with the floating wind turbine system alone for the Pantelleria case study. The energy produced from each device is obtained as

$$E_p = \sum_{i=1}^{N} P_i(H_s, T_e, V_0) \cdot O_i(H_s, T_e, V_0) \qquad (31)$$

where P_i and O_i are the power and the occurrence of each environmental condition and N is the number of triplets.

2.4 Techno-economic analysis

The CAPital Expenditure (CAPEX) (C_0) of the hybrid device is calculated as

$$C_0 = C_{WT} + C_p + C_M + C_{Inst} + C_{cables} + C_{PTO}, \qquad (32)$$

where C_{WT} is the cost of the wind turbine, C_M is the mooring cost, C_{Inst} is the installation cost and C_{cables} are the costs due to the marine cables (See Table 6). The platform cost (C_p) of Eq. (24) is updated in this analysis to account also for the manufacture process for more accurate estimation (manufacture cost factor is assumed 1.5).

C_M is calculated as

$$C_M = n_M \cdot (C_{Anchor} + c_M \cdot L_M), \qquad (33)$$

where L_M is the mooring length and n_M is the number of mooring lines.

C_{cables} is obtained as

$$C_{cables} = L_{Array} \cdot (C_{FarmCab} + C_{FarmLay}) \cdot n_t + L_{Ex} \cdot (C_{SubCab} + C_{SubLay}), \qquad (34)$$

where L_{Array} and L_{Ex} are the distances between the wind turbines in the farm (0.5 km) and from the offshore to the onshore substations (10 km). $C_{FarmCab}$ (481 €/m), $C_{FarmLay}$ (1500 €/m), C_{SubCab} (668 €/m) and C_{SubLay} (275 €/m) are the costs of the marine cables and of laying process for the wind farm and between the substations. n_t is the number of devices which is considered as 10 in this study.

Table 6 Techno-economic assumptions

Wind turbine	1.3 M€/MW (Fundació Institut de Recerca en Energia de Catalunya 2015)
Moorings (c_M)	500 £/m (James and Ros 2015)
Anchors (C_{Anchor})	200 M£/unit
Marine cables	400–800 €/m (7 Seas Med srl 2022)
Installation	0.15 M£/MW (James and Ros 2015)

The LCOE is expressed as

$$\text{LCOE} = \frac{C_0 + \sum_{i=1}^{n} \frac{O}{(1+r)^i} + \frac{D}{(1+r)^n}}{\sum_{i=1}^{n} \frac{E}{(1+r)^i}}, \tag{35}$$

where O, D and E are the Operating Expenditure (OPEX), the decommissioning cost and the annual energy production for the offshore wind farm; r is the Weighted Average Cost of Capital (WACC), and n is the project lifetime. The OPEX is estimated as 0.2 M€/MW, whilst decommissioning cost is estimated as 2% of total CAPEX (James and Ros 2015). The WACC is assumed 8%, whilst the project lifetime is assumed 25 years.

3 Results

3.1 Optimal design geometry

The float geometry has been optimised for three different shapes and several design parameters to minimise the objective function described in Eq. 24. The semi-cylindrical and cylindrical shapes include three geometry design parameters, whilst the spherical shape includes only two. For all geometries, the spring and the damping parameters of the PTOs are also optimised to maximise the power generated by the WECs and ensure that the dynamic constraints are met. Convergence of the objective function has been checked by comparing the results of two different optimisations for each geometry (see Fig. 8a). The number of optimisations for each geometry has been limited due to the high computational effort required for the optimisations (2–3 days each with 4 parallel workers using the MATLAB function *parfor*). Optimal values are generally obtained for the semi-cylindrical and cylindrical shapes whilst the spherical shape converge to larger values. A worse optimal configuration for the spherical shape compared to the other ones could be related to fewer geometry parameters and a less effective hydrostatic stiffness response due to the relative position with the waterplane area. The semi-cylindrical and the cylindrical configurations converge to similar optimal values, with the cylindrical optimal shape slightly outperforming the semi-cylindrical shape

(Cyl2 and SemiCyl1). The optimal arm length generally converges towards the lowest value considered for all shapes. The optimal cylindrical shape has the largest radius and smallest height in the design parameter range, as shown in Fig. 8b, whilst the semi-cylindrical shape converges to the largest height. The structure mass is mainly due to the concrete, the material chosen for the floats to ensure a null net hydrostatic torque at each arm hinge (see Table 7). The steel and ballast masses are generally less than 1000 tonnes, which is at least three times less than the concrete masses.

Finally, Fig. 9 shows the main time domain results for Cyl2, which include the pitch platform and nacelle acceleration (dynamic constraints of the optimisation), the mean power of the WECs and the wind turbine, and the environmental conditions of the simulation (wave elevation and wind speed at rotor height). Most of the power of the WECs comes from WEC1, which is around 10 times larger than the other two WECs at the rear of the device. WEC2 and WEC3 produced the same power during the simulation due to their symmetry relative to the wind and wave direction. The power of the WECs shows strong fluctuations, which could cause difficulties in a more detailed design of the power take-off. For this reason, a hydraulic PTO was selected to allow hydraulic storage smoothing the generated power and will be investigated in the next section. The frequency domain results of the motion of platform and the WECs are also shown in Fig. 9d, e. Figure 9d represents the power spectral density of the motion of the optimisation triplet ($H_s = 6$ m, $T_e = 7$ s and $V_0 = 11$ m/s) whilst Fig. 9e shows the Response Amplitude Operators (RAOs) obtained simulating the device for 100 regular waves along the wave frequency range and a wind speed of 11 m/s for the optimal PTO setting of Cyl2. Main motion response of the device of the optimisation triplet is as expected next to the energy and peak period of the simulation (7–8 s) as shown in Fig. 9d. The RAOs of the platform and WECs show mainly surge resonance for large periods due to the large size of the device along this dimension, heave resonance around 5 s and high periods and pitch resonance about 9–10 s as shown in Fig. 9e.

PTO results of Cyl2 have been analysed to investigate the technical feasibility of the configuration in Fig. 10. Figure 10 shows the time domain results of the PTO angular motion (θ), cylinder stroke, PTO torque, PTO and radial bearing forces. These results are checked for the most critical PTO, the front one (PTO1), which is characterised by the largest PTO force and power. PTO angular motion is limited to small angles (less than 12°), resulting in a piston stroke that is also limited to sensible values of less than 400 mm (TLP 2022). The reduced stroke of the piston is determined by the large stiffness and damping coefficients of the optimal linear PTO design configuration. This results in a large PTO force, which is about 4 times larger than the maximum available design specification of this component from TLP
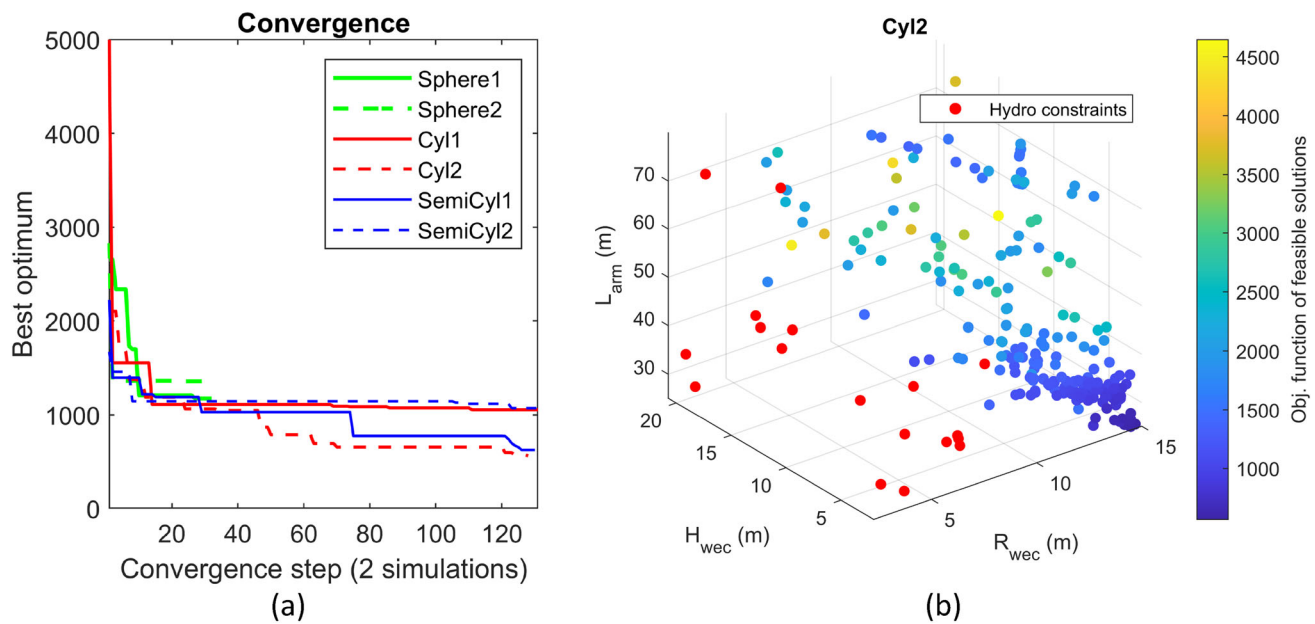
Fig. 8 Optimisation convergence for the different shapes of the WEC (**a**) and convergence of the geometry design parameters for the cylindrical shape (**b**)

Table 7 Optimal results for the different optimisations

	Sphere1	Sphere2	Cyl1	Cyl2	SemiCyl1	SemiCyl2
R_{wec} (m)	12.17	14.39	10.43	14.89	3.96	6.72
H_{wec} (m)	–	–	13.68	2.39	49.74	24.12
L_{arm} (m)	40.77	32.20	26.72	25.17	26.61	31.43
k_{PTO} (MNm/rad)	1500.90	2028.50	417.45	332.98	151.11	332.98
c_{PTO} (MNMs/rad)	1305.37	2900.62	451.80	1300.63	2065.60	1232.18
Mean WECs power (MW)	3.44	4.16	2.60	2.58	2.63	1.73
Mean wind power (MW)	3.61	3.64	3.66	3.72	3.65	3.59
Max platform pitch (deg)	14.94	12.74	12.51	8.09	10.68	14.41
Rms nacelle acceleration (m/s^2)	1.99	1.78	0.91	1.44	1.90	1.42
Max static pitch angle (deg)	4.96	6.89	3.57	1.60	2.29	2.52
Thickness WECs (m)	2.04	2.43	1.36	0.26	0.48	0.77
Steel mass (tonne)	1011.68	921.41	828.35	791.24	868.69	898.53
Concrete mass (tonne)	23,021.11	38,230.69	13,304.50	2968.91	3699.68	5190.13
Ballast mass (tonne)	589.72	626.85	697.65	711.84	703.46	672.40
Objective function (–)	1175.33	1359.48	1036.03	565.63	627.68	1073.66

(2022). Therefore, the PTO hydraulic solution will require a very large piston area (e.g. 0.3–0.5 m^2) and working pressure (1000–2000 MPa) to withstand these loads. The PTO hydraulic solution must be carefully designed to avoid an unfeasible design solution and is carefully addressed in the next Sect. 3.2. Finally, the maximum radial bearing force is about 10 MN, which gives option to several bearing design solutions (ZWA Bearings 2023) (see Fig. 10b).

3.2 Optimal hydraulic PTO configuration

The main parameters of the hydraulic PTOs were optimised for the optimal geometry configuration Cyl2 for a hydraulic motor rated power of 150 kW for each WEC. The results of the optimisation are shown in Fig. 11 and Table 8. In particular, the optimal hydraulic PTO parameters are found for large piston areas and LPA pre-charge pressures whilst the
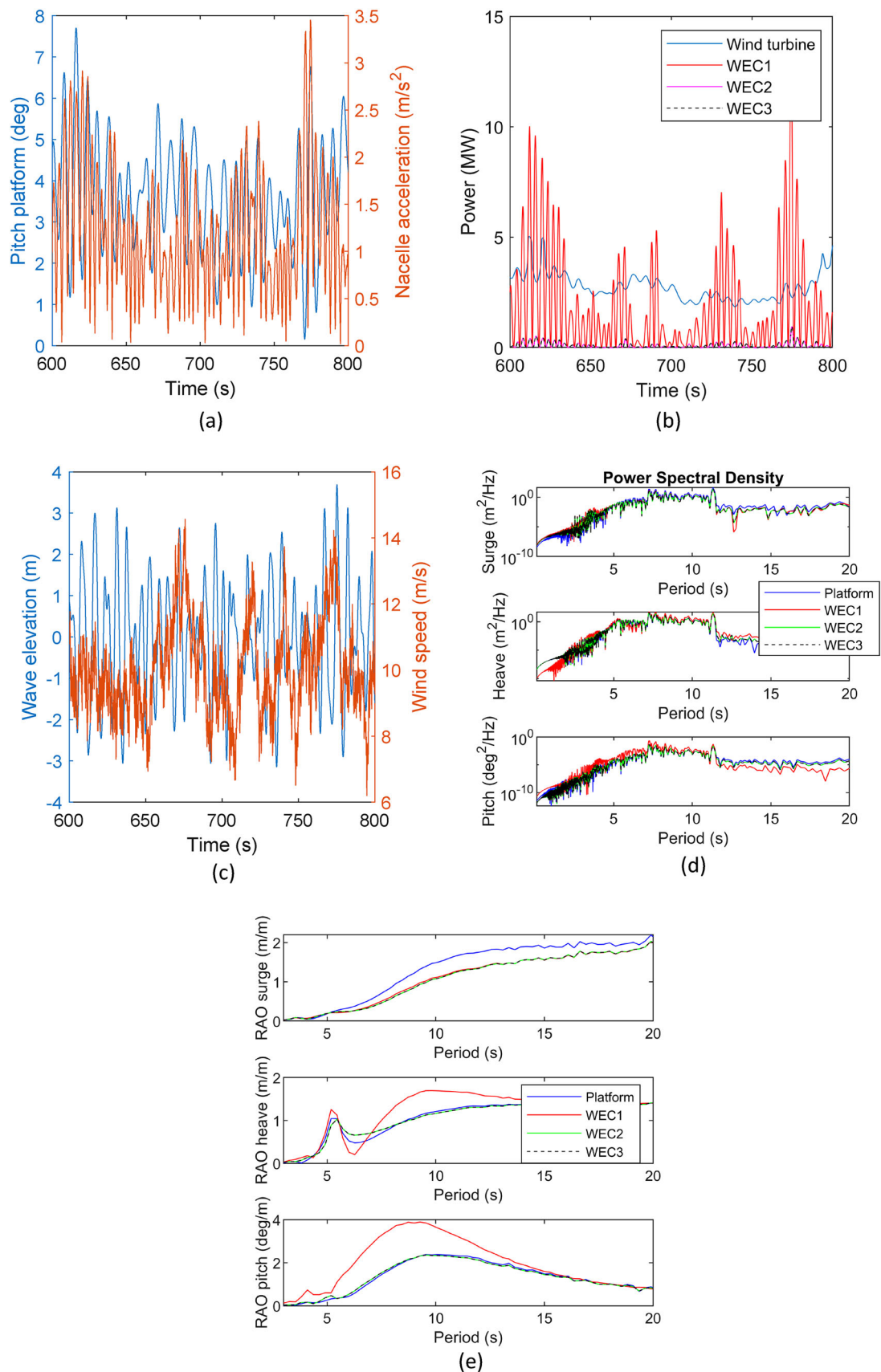
Fig. 9 Pitch platform and nacelle acceleration (**a**), WECs and wind turbine power (**b**), wave elevation and speed (**c**), power spectral density of motion of platform and WECs (**d**) of the optimisation triplet and RAOs of the platform and WECs (**e**) for Cyl2
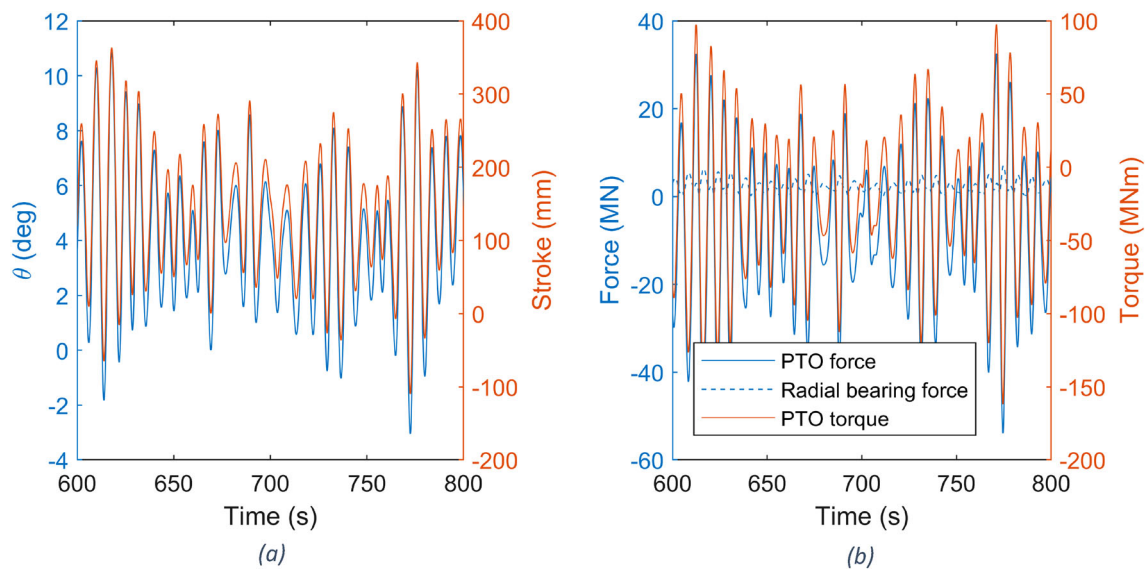
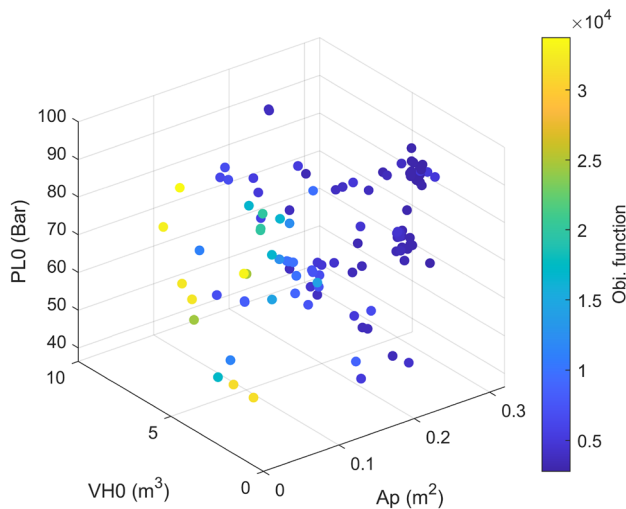**Fig. 10** PTO1 results including PTO angular motion and piston stroke (**a**), PTO force, PTO torque and radial bearing force (**b**) of Cyl2

Fig. 11 Convergence of the Hydraulic PTO

Table 8 Optimal results including the hydraulic PTO

Piston area (m^2)	0.3
HPA volume (m^3)	3.63
LPA volume (m^3)	0.5
LPA pre-charge pressure (MPa)	8.62
Mean Abs/Mech/El WECs power (MW)	0.67/0.64/0.53
Abs. power fluctuation ratio for PTO1/2/3 (–)	25.18/5.35/5.31
El. power fluctuation ratio for PTO1/2/3 (–)	8.02/2.47/2.45
Mean wind power (MW)	3.70
Max platform pitch (deg)	8.57
Rms nacelle acceleration (m/s^2)	1.67
Objective function (–)	2782.7

optimal HPA volume converges in the middle range considered. Optimal large values of the HPA volume are especially limited by the objective function imposing a cost on the HPA volume. It is important to check the ratio of power fluctuations (the instantaneous power can be an order of magnitude greater than the average power (Yu et al. 2018)), as it must be sufficiently low for optimal survival of the hydraulic PTO and lower costs. Electrical power fluctuation ratio is reduced by more than half compared to the absorbed power fluctuation ratio and it reaches sensible values also for power grid supply. Power conversion efficiency from absorbed to electrical power is also relatively high (78%) compared to other studies (e.g. Amini et al. 2022). Maximum platform pitch and rms nacelle acceleration are similar to the optimal results obtained with the linearized PTO of Cyl2. However, an additional PTO rotational spring of 500 MNm/rad like the linearized model was included, as the hybrid device was otherwise unable to withstand especially the wind loads whilst maintaining the dynamic constraints. It is foreseen that the implementation of a more efficient hydraulic PTO (e.g. a discrete displacement hydraulic PTO) capable of integrating the spring response will cancel the need of these additional components.

Figure 12 shows the main results of the optimal configuration of the hydraulic parameters in the time domain. The results prove to be sensible in comparison with the available technical details of the components on the market, such as the double-acting hydraulic piston pump (TLP 2022), the variable displacement hydraulic motor (Liehberr 2022) and the accumulators (Hydac 2022). The power generated by the front PTO (PTO1) is greater than that of the rear PTO (PTO2 and PTO3), similar to the results of the linearised PTO (see Fig. 12b). However, the ratio between their average powers is
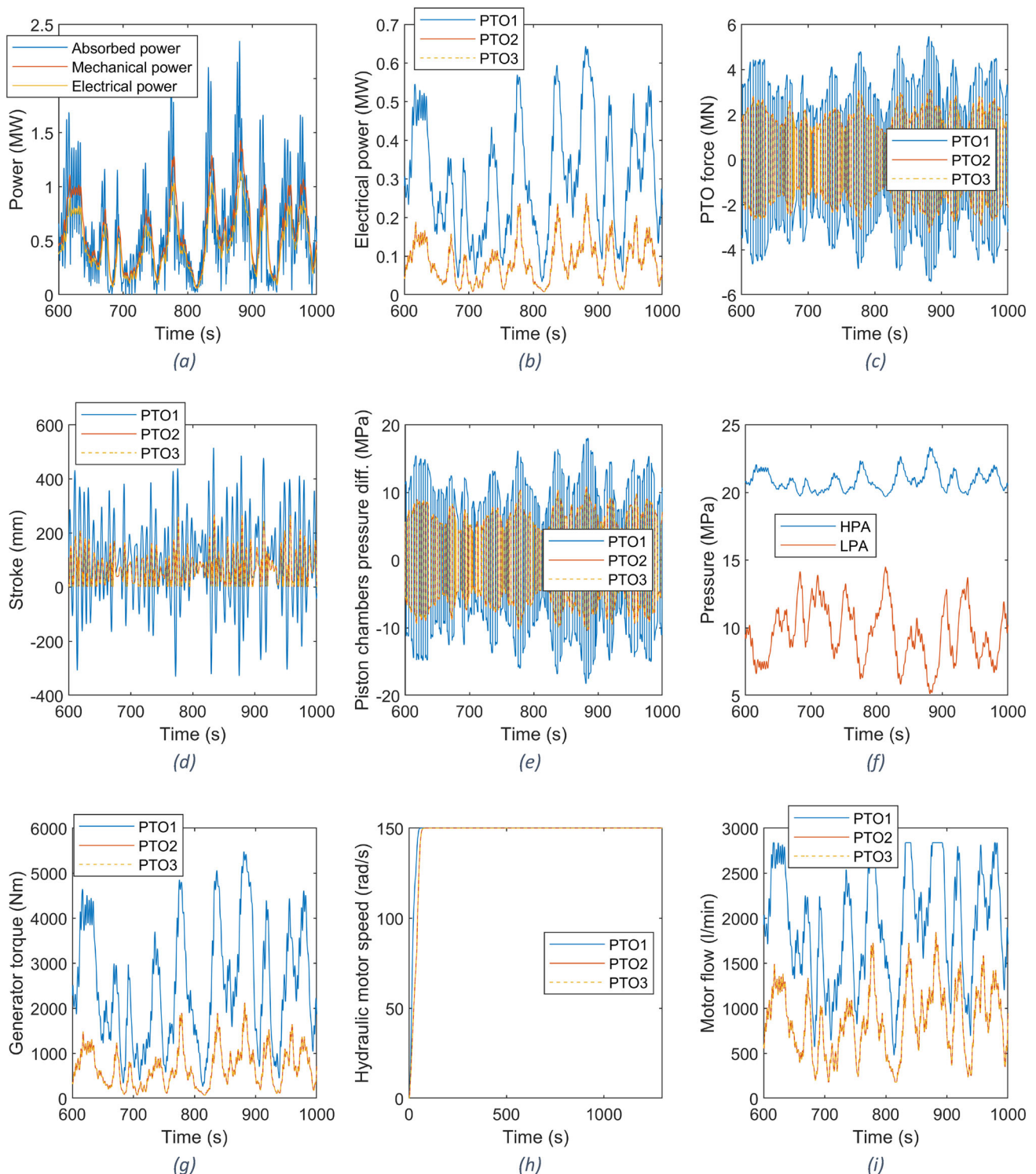
Fig. 12 Time domain results of the main outputs of the optimal hydraulic PTO configuration

lower than before (about 4). The speed of the hydraulic motor reaches the nominal value very fast at the beginning of the simulation (see Fig. 12h). The maximum piston PTO force and the stroke are less than 6 MN and 600 mm respectively as shown in Fig. 12c, d.

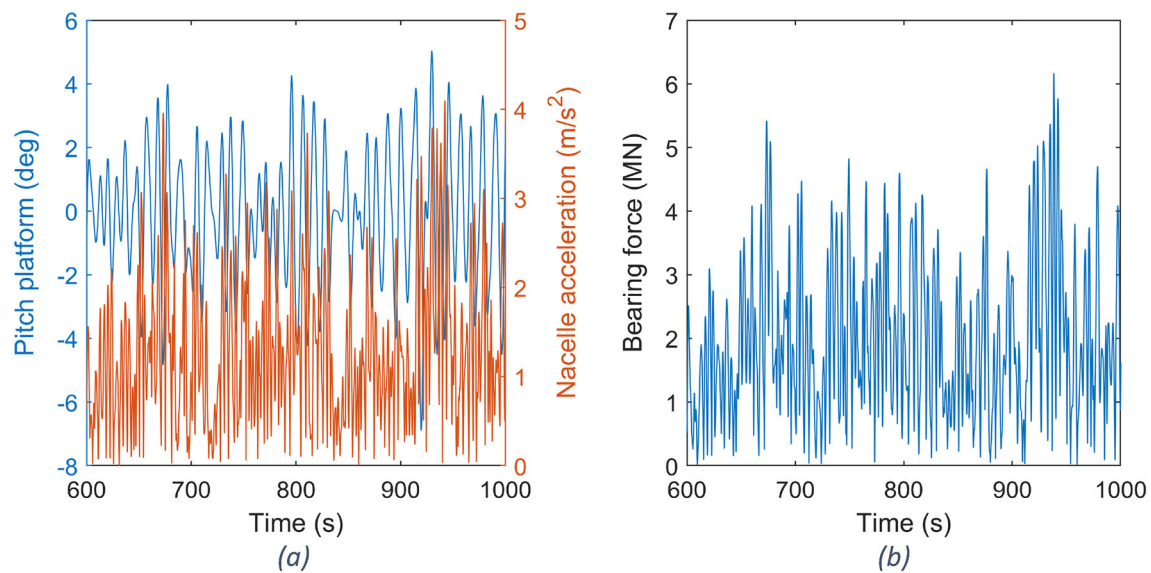Dynamic performance of the optimal design configuration and bearing force on PTO1 are checked for the extreme

Fig. 13 Dynamic performance and bearing for check on PTO1 for the extreme environmental condition (Hs = 7.33 m, Te = 9.89 s and V_0 = 26.14 m/s)

environmental conditions described in Sect. 2.2.4. Relative position between arms and central cylinder is fixed and PTOs are in survival mode as described in Sect. 2.1. Wind speeds are above the cut-off speed and the wind turbine is therefore not operating. In this condition, the aerodynamic loads accounted in the simulation are the drag on the blades and tower and will be much smaller than during operating. A maximum platform pitch of 8.48° and a rms nacelle acceleration of 1.72 m/s^2 are obtained for the largest H$_S$ extreme environmental condition which demonstrates that the hybrid system structural integrity is maintained (see Fig. 13). Bearing radial force on PTO1 is below 10 MN similar to the results of Sect. 3.1.

3.3 Comparison between hybrid and wind floating system

The floating wind turbine has been compared with the hybrid device to investigate the techno-economic potential of the novel concept. The hybrid concept is included in the comparison with the hydraulic PTO and the linear PTO. The hydraulic PTO represents a more realistic PTO configuration which, however, can be still improved choosing a different type of hydraulic PTO (e.g. discrete displacement hydraulic PTO) and a control algorithm (e.g. reactive, MPC, latching, and declutching). The hybrid device with hydraulic PTOs is used with same optimised PTO parameters from previous Sect. 3.2 for all triplets. PTO parameters of the linear PTOs (k_{PTO} and c_{PTO}) are instead optimised for each triplet. Figure 14 compares the pitch, nacelle acceleration and power for all triplets considered as described in Sect. 2.2.4. The triplets are ordered based on their wave energy content whilst the wind speed

varies along them. The floating wind turbine shows a better dynamic stability compared to the hybrid device for less energetic wave energy triplets whilst similar dynamic stability is obtained for the most energetic triplets. It is important to remind that the hybrid device has not been optimised to improve dynamic stability but only to respect dynamic constraints which demonstrate a lower performance compared to the floating wind turbine. Dynamic constraints of the optimisation are not verified for the most energetic triplets for the floating wind and the hybrid device with hydraulic PTOs. However, the hybrid device with linear PTOs demonstrates that the WECs can be used to respect the constraint limits and at the same time produce wave energy power. Mean power of hybrid device has an impact on the total device extracted power only for the most energetic triplets as shown in Fig. 14b, which reduces the significance of the WECs for wave energy extraction in low sea conditions.

Mean power from WECs is around 2.6% and 7% compared to mean power from the wind turbine for the hybrid device with hydraulic and linear PTOs respectively as shown in Table 9. Safety locks between WECs arms and central cylinder have been also added to the hybrid device total cost and are assumed equal to the WEC arms cost. LCOE of the hybrid device can be theoretically reduced by 11% compared to the floating wind turbine when WECs PTO loading is assumed linear and commercial cost assumptions for the hydraulic PTO are made. LCOE reduction of the hybrid is due to the added power production of the WECs (7.49%) and the power increase of the wind turbine (6.76%) compared to the floating wind turbine device. The rated power of the linear PTOs is assumed to be about three times the average power (450 kW each) to obtain a similar ratio to the hydraulic PTO
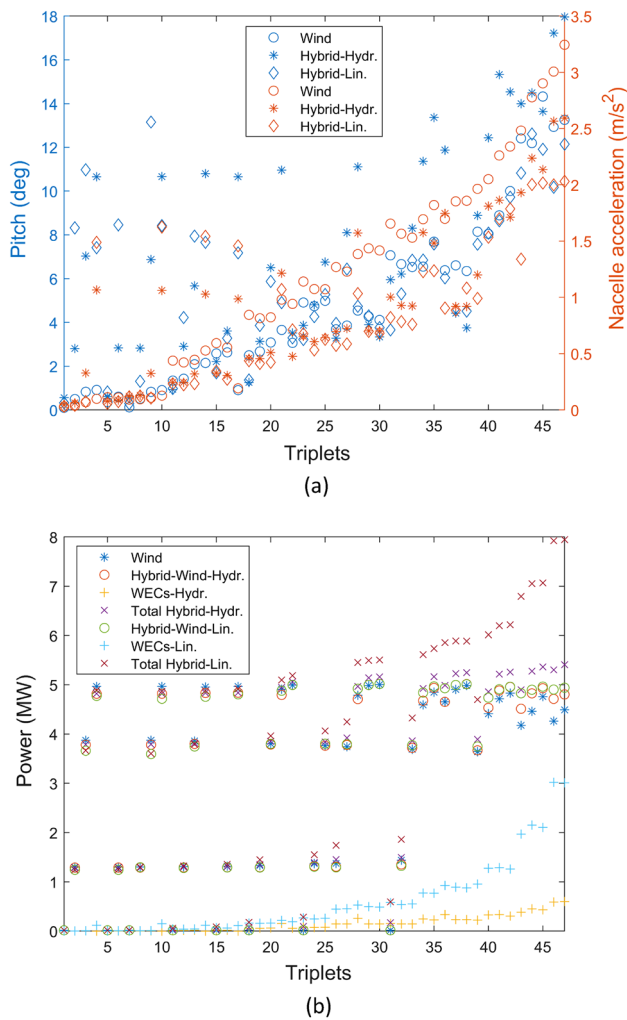
Fig. 14 Pitch and nacelle acceleration (**a**) and mean power (**b**) of wind floating system, hybrid with hydraulic PTOs and hybrid with linear PTOs

Table 9 Techno-economic comparison between floating wind and hybrid (Hydr. + Linear)

	Only wind	Hybrid hydr	Hybrid lin
Mean wind power (MW)	2.338	2.379	2.496
Mean wave power (MW)	–	0.061	0.175
Total power (MW)	2.338	2.440	2.671
Rated power (MW)	5	5.45	5.9
Capacity factor (%)	46.76	44.77	45.27
Wind turbine cost (M€)	65.00	65.00	65.00
Platform steel cost (M€)	35.61	35.61	35.61
Platform concrete cost (M€)	11.13	11.13	11.13
Platform ballast cost (M€)	0.85	0.85	0.85
Safety locks (M€)	–	0.30	0.30
Hydraulic PTO pro-totypal/industrial (M€)	–	23.64/1.53	47.09/4.59
Marine cables cost (M€)	19.34	19.34	19.34
Mooring cost (M€)	24.63	24.63	24.63
Installation cost (M€)	10.33	10.33	10.33
Decommissioning (M€)	3.34	3.83/3.37	4.29/3.44
LCOE wind (€/MWh)	126.69	132.09/122.21	130.25/112.89

Mean power is referred to a single wind turbine whilst the costs are referred to the wind farm

4 Discussion

In this work, an optimal design configuration of a novel hybrid concept designed to survive severe metocean conditions whilst maximising the energy generated by the WECs was identified. The optimal design configuration is mainly influenced by cost, as most optimisations converge near the shortest arm (e.g. cylindrical and semi-cylindrical optimisations). The selected configuration is the cylindrical configuration which has the shortest height and the largest radius from the design parameter range considered. This design configuration needs to be structurally verified and requires a more detailed design to determine a possible feasible solution of the design (e.g. structural frame of the arms). The structural integrity of the floats can be verified with a FEM analysis that identifies critical structural locations that are affected by hydrodynamic loads (Campos et al. 2017).
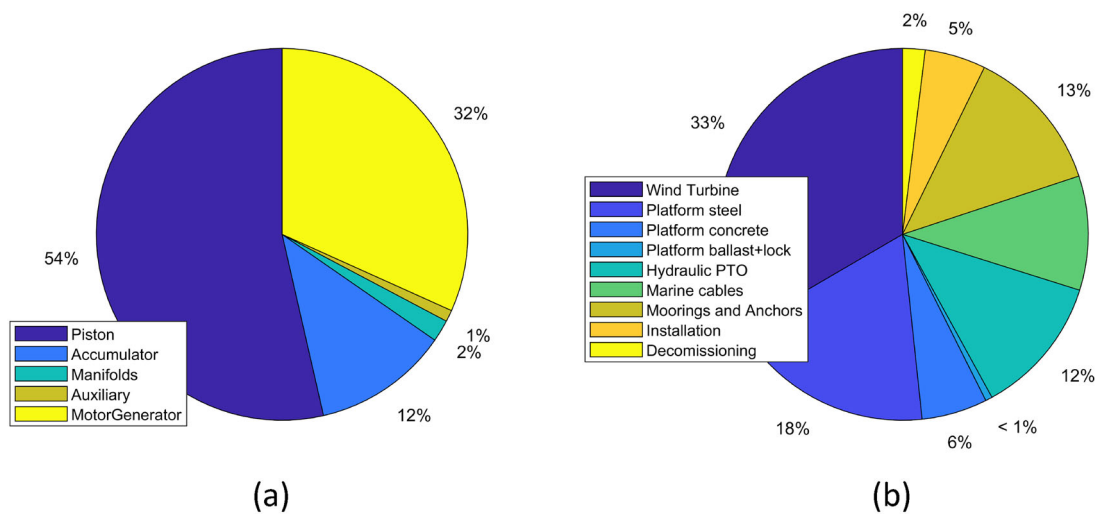
case, whilst the piston area is assumed to be 0.5 m^2 to account for the higher costs due to the larger PTO forces investigated in Sect. 3.1. Costs are mainly due to the wind turbine and the steel platform (49%) as shown in Fig. 15. Then marine cables and mooring costs also play a significant role in the total cost. The PTO cost from the WECs significantly influences the overall cost (about 12%) if conceptual assumption is made. Hydraulic PTO cost is mainly related to the primary PTO and especially to the piston component (54%) as shown in Fig. 15a due to the large piston area selected for the optimal hydraulic PTO configuration (0.3 m^2).

Fig. 15 Pie chart for the hydraulic PTO costs (**a**) and hybrid device cost components with PTO of WECs estimated at conceptual stage (**b**)

Fatigue and ultimate loads can be then determined to verify the safety limits (Shahroozi et al. 2022).

The case study of Pantelleria was chosen as it is an energetic location in the Mediterranean Sea with high wind and wave energy potential. However, WECs at this site have shown low efficiency, so more energetic sites on the Atlantic coast (e.g. Belmullet, Wave Hub) also need to be considered. At these sites, the wave power density could be more than 10 times higher and the WECs could make a larger contribution to the total energy production. On the other hand, the WECs could be used to improve the dynamic stability of the platform in Pantelleria, thus reducing the overall cost of the structure.

The power from the WECs is mainly generated by the WEC at the front for wind and waves with the same and a single direction. The other two WECs could play a more significant role in power generation when other wave directions are considered. A sensitivity analysis of the device with wind and wave direction is required to fully understand the amount of power from each WEC. The amount of energy generated by the WECs reaches 7% compared to the energy of the wind turbine, which is in line with the WindWEC study (Karimirad and Koushan 2017) (6%).

The hydraulic PTO of this work is a variable displacement hydraulic motor optimised based on three PTO design variables. The PTO could be further improved, e.g. by changing the control law relating the motor flow and the pressure difference between the accumulators for different metocean conditions (Eq. (20)). The amount of energy of the hybrid system with hydraulic PTO is also significantly (about three times) reduced compared to the system with linear PTO. The main reason for this is that the hydraulic PTO is operated with the same settings in all configurations, whilst reactive control

is implemented for the linear PTOs. Improved power generation of the hydraulic PTOs could also be achieved using discrete displacement cylinders (Henderson 2006), which would allow optimal loading of the control manifold. This type of PTO could be optimised to produce a similar amount of energy compared to reactive control. Furthermore, this PTO could provide an additional stiffness load on each arm which was required in addition to the hydraulic PTOs of this study to keep the floating structure dynamically stable from wind loads. Other types of control which will need to be investigated are the latching control and the declutching controls as well as Model Predictive Control (MPC) (Quartier 2018).

5 Conclusion

In this paper, an optimal design for a novel wind and wave hybrid concept was investigated. The hybrid concept consists of a floating wind turbine with three WECs to increase the power generated by the turbine and to ensure the floating stability of the platform. The optimal WEC geometry is a cylindrical structural shape with the largest radius and lowest height, which has better performance compared to the semi-cylindrical and spherical shapes. The optimisation was performed using the genetic algorithm in combination with the Kriging surrogate model, checking the convergence of the optimisation for each geometry. The numerical model is based on open-source and in-house software which computes the hydrostatic and time domain results of the hybrid platform configuration, checking simulation constraints, such as the static and maximum dynamic pitch angles and the maximum rms of nacelle acceleration. The case study selected is Pantelleria as it is an energetic wind and wave location in the

Mediterranean Sea. For the design optimisation of the WECs, a single triplet is chosen to represent the severe metocean conditions in power production region. 47 triplets were chosen for the estimation of the annual energy production in Pantelleria. The hybrid system is compared to the floating wind system and is shown to be a potentially better solution with a LCOE reduction up to 11%, based on commercial assumptions for the hydraulic PTO estimation. Power increase of the hybrid design is about 14.3% (7.5% from WECs and 6.8% from wind turbine). The power generated by WECs is significantly reduced (by about three times) when power is estimated by hydraulic PTOs instead of linear PTOs, as the power of linear PTOs has been optimised for each metocean condition (reactive control). However, a hydraulic PTO is recommended to reduce the power fluctuation ratio and to store the energy produced in the accumulators for a smoother power production. The survival conditions of the hybrid device are respected with a maximum dynamic pitch of 8.48°, whilst operating conditions show a maximum stroke, bearing and PTO forces less than 600 mm, 10 MN and 6 MN respectively.

Further work will include the investigation of other types of hydraulic power take-offs, such as the hydraulic power take-offs with discrete displacement cylinders, where reactive control is possible. The power from the WECs in the rear of the device demonstrated low performance. Therefore, the hybrid device will be tested in different wind and wave directions to see if the rear WECs play a more important role or if a hybrid structure with a single front WEC is more suitable.

Availability of data and materials Not applicable.

Declarations

Conflict of interest The authors declare no potential conflicts of interest with respect to the research, authorship and/or publication of this article.

Ethical approval Not applicable.

References

Acciona (2015) MARINA. CORDIS EU research results. https://cordis.europa.eu/project/id/241402. Accessed 11 Aug 2023

Amini E, Mehdipour H, Faraggiana E, Golbaz D, Bracco GMS, Neshat M (2022) Optimization of hydraulic power take-off system settings for point absorber wave energy converter. Renew Energy 194:938–954. https://doi.org/10.1016/j.renene.2022.05.164

Babarit A, Gérard D (2015) Theoretical and numerical aspects of the open source BEM solver NEMOH. In: 11th European wave and tidal energy conference (EWTEC2015). Nantes

Bonfanti M (2021) Mixing the power of water and oil. Doctoral Dissertation, Politecnico di Torino

Campos A, Molins C, Trubat P, Alarcón D (2017) A 3D FEM model for floating wind turbines support structures. Energy Procedia 137:177–185. https://doi.org/10.1016/j.egypro.2017.10.344

Chozas JF, Kofoed JP Jensen NEH (2014) User guide—COE calculation tool for wave energy converters: ver. 1.6—April 2014. DCE Technical reports no. 161. Department of Civil Engineering, Aalborg University, Aalborg. https://vbn.aau.dk/ws/portalfiles/portal/197329237/User_guide_to_the_COE_Calculation_Tool_ver1.6_April2014.pdf. Accessed 17 Aug 2023

Danmarks Tekniske Universitet (2014) Deliverable D4.3.3—innovative concepts for floating structures. INNWIND.EU. http://www.innwind.eu/publications/deliverable-reports. Accessed 17 Aug 2023

DNV (2010) RP-C205: environmental conditions and environmental loads. DNV. https://rules.dnv.com/docs/pdf/dnvpm/codes/docs/2014-04/RP-C205.pdf. Accessed 17 Aug 2023

DNV-GL (2018) ST-0119: floating wind turbine structures. DNV. https://www.dnv.com/energy/standards-guidelines/dnv-st-0119-floating-wind-turbine-structures.html. Accessed 17 Aug 2023

ECMWF (2022) ERA5. Copernicus EU. https://cds.climate.copernicus.eu/cdsapp#!/dataset/reanalysis-era5-single-levels?tab=overview. Accessed 17 Aug 2023

EDF Energy (2023) Salome-meca. Codeaster. http://www.code-aster.org/spip.php?article303. Accessed 10 Aug 2023

Faraggiana E, Chapman JC, Williams AJ, Masters I (2020) Genetic based optimisation of the design parameters for an array-on-device orbital motion wave energy converter. Ocean Eng 218:108251. https://doi.org/10.1016/j.oceaneng.2020.108251

Faraggiana E, Chapman JC, Williams AJ, Whitlam C, Masters I (2022a) Investigation of new layout design concepts of an array-on-device WaveSub device. Renew Energy 190:501–523. https://doi.org/10.1016/j.renene.2022.03.126

Faraggiana E, Sirigu M, Ghigo A, Bracco G, Mattiazzo G (2022b) An efficient optimisation tool for floating offshore wind support structures. Energy Rep 8:9104–9118. https://doi.org/10.1016/j.egyr.2022.07.036

Faraggiana E, Sirigu M, Ghigo A, Bracco G, Mattiazzo G (2022c) An optimal design of the Hexafloat floating platform for offshore wind turbines. Trends in renewable energies offshore, RENEW 2022 conference. CRC Press, Lisbon, pp 469–476

Fenu B, Attanasio V, Casalone P, Novo R, Cervelli G, Bonfanti M, Sirigu SA, Bracco G, Mattiazzo G (2020) Analysis of a gyroscopic-stabilized floating offshore hybrid wind-wave platform. J Mar Sci Eng 8(6):439

Floating Power Plant Ltd (2017) Poseidon. CORDIS EU research results. https://cordis.europa.eu/project/id/673976. Accessed 11 Aug 2023

Fraunhofer-Gesellschaft (2011) ORECCA. CORDIS EU research results. https://cordis.europa.eu/project/id/241421. Accessed 11 Aug 2023

Fundació Institut de Recerca en Energia de Catalunya (2015) Deliverable 2.2. LCOE tool description, technical and environmental impact evaluation procedure. LIFES50+ project. https://lifes50plus.eu/results/. Accessed 17 Aug 2023

Ghafari HR, Ghassemi H, He G (2021) Numerical study of the Wavestar wave energy converter with multi-point-absorber around DeepCwind semisubmersible floating platform. Ocean Eng 232:109177. https://doi.org/10.1016/j.oceaneng.2021.109177

Green Ocean Energy (2023) Wave treader. Renewable technology. https://www.renewable-technology.com/projects/green-ocean-wave-treader/. Accessed 11 Aug 2023

Hainsch K, Brauers H, Burandt T, Goeke L, von Hirschhausen CR, Kemfert C, Kendziorski M, Löffler K, Oei PY, Präger F, Wealer B (2020) Make the European Green Deal real: combining climate neutrality and economic recovery. DIW Berlin: Politikberatung kompakt, Berlin. http://hdl.handle.net/10419/222849. Accessed 17 Aug 2023

Hanssen JE, Margheritini L, O'Sullivan K, Mayorga P, Martinez I, Arriaga A, Agos I, Steynor J, Ingram D, Hezari R, Todalshaug JH (2015) Design and performance validation of a hybrid offshore renewable energy platform. In: Tenth international conference on ecological vehicles and renewable energies (EVER). Monaco, pp 1–8

Henderson R (2006) Design, simulation, and testing of a novel hydraulic power take-off system for the Pelamis wave energy converter. Renew Energy 31:271–283. https://doi.org/10.1016/j.renene.2005.08.021

Hydac (2022) High pressure bladder accumulators. Hydac. https://www.hydac.com/shop/en/hydraulic-accumulators. Accessed 4 Nov 2022

James R, Ros MC (2015) Floating offshore wind: market and technology review. The carbon trust. https://www.carbontrust.com/our-work-and-impact/guides-reports-and-tools/floating-offshore-wind-market-technology-review. Accessed 17 Aug 2023

Jonkman BJ, Buhl Jr ML (2006) TurbSim user's guide. National Renewable Energy Lab, Golden, CO (United States). https://www.nrel.gov/docs/fy06osti/39797.pdf. Accessed 17 Aug 2023

Jonkman J, Butterfield S, Musial W, Scott G (2009) Definition of a 5-MW reference wind turbine for offshore system development. National Renewable Energy Lab, Golden, CO (United States). https://www.nrel.gov/docs/fy09osti/38060.pdf. Accessed 17 Aug 2023

Karimirad M (2014) Offshore energy structures: for wind power, wave energy and hybrid marine platforms. Springer, London

Karimirad M, Koushan K (2017) WindWEC: combining wind and wave energy inspired by hywind and wavestar. In: IEEE international conference on renewable energy research and applications, ICR-ERA 2016. Birmingham

Lee J, Zhao F (2021) GLOBAL OFFSHORE WIND REPORT 2021. Global Wind Energy Council, Brussels. https://gwec.net/global-offshore-wind-report-2021/. Accessed 17 Aug 2023

Li L, Gao Y, Yuan Z, Day S, Hu Z (2018) Dynamic response and power production of a floating integrated wind, wave and tidal energy system. Renew Energy 116:412–422. https://doi.org/10.1016/j.renene.2017.09.080

Liehberr (2022) Variable displacement hydraulic motor. Liehberr. https://www.liebherr.com/en/int/products/components/hydraulics/hydraulic-pumps-and-motors/axial-piston-motors-adjustable/details/dmvadoppelmotor.html. Accessed 4 Nov 2022

Luan C, Michailides C, Gao Z, Moan T (2014) Modeling and analysis of a 5 MW semi-submersible wind turbine combined with three flap-type wave energy converters. In: 33rd International conference on

offshore mechanics and arctic engineering. American Society of Mechanical Engineers, San Francisco, p V09BT09A028

Marquis L, Kramer M, Kringelum J, Chozas JF, Helstrup NE (2012) Introduction of Wavestar wave energy converters at the Danish offshore wind power plant Horns Rev 2. In: 4th International conference on ocean energy. Dublin

Masciola M (2018) MAP++ Documentation. NREL. https://map-plus-plus.readthedocs.io/en/latest/index.html. Accessed 11 Aug 2023

McTiernan KL, Sharman KT (2020) Review of hybrid offshore wind and wave energy systems. In: NAWEA WindTech 2019. Journal of Physics: Conference Series, Amherst, Massachusetts, p 12016

Michailides C, Gao Z, Moan T (2016) Experimental study of the functionality of a semisubmersible wind turbine combined with flap-type Wave Energy Converters. Renew Energy 93:675–690. https://doi.org/10.1016/j.renene.2016.03.024

Muliawan MJ, Karimirad M, Moan T (2013) Dynamic response and power performance of a combined spar-type floating wind turbine and coaxial floating wave energy converter. Renew Energy 50:47–57. https://doi.org/10.1016/j.renene.2012.05.025

Pecher A, Kofoed JP (2017) Handbook of ocean wave energy. Springer, London

Pérez-Collazo C, Greaves D, Iglesias G (2015) A review of combined wave and offshore wind energy. Renew Sustain Energy Rev 42:141–153. https://doi.org/10.1016/j.rser.2014.09.032

Petracca E, Faraggiana E, Ghigo A, Sirigu M, Bracco G, Mattiazzo G (2022) Design and techno-economic analysis of a novel hybrid offshore wind and wave energy system. Energies 15:2739. https://doi.org/10.3390/en15082739

PLOCAN (2015) TROPOS. CORDIS EU research results. https://cordis.europa.eu/project/id/288192. Accessed 11 Aug 2023

Quartier N (2018) Numerical implementation of the power-take-off (PTO) of two types of generic wave energy converters using WEC-Sim. Master's Dissertation, Ghent University

Roddier D, Cermelli C, Aubault A, Weinstein A (2010) WindFloat: a floating foundation for offshore wind turbines. J Renew Sustain Energy 2:33104. https://doi.org/10.1063/1.3435339

Sea For Life (2022) Marine technology firm Sea For Life introduces WEGA ocean energy device. Hydro Review. https://www.hydroreview.com/hydro-industry-news/marine-technology/#gref. Accessed 5 Dec 2022

7 Seas Med srl (2022) Environmental evaluations and authorizations. Italian Ministry of the Environment and Land and Sea Protection. https://va.minambiente.it/it-IT/Oggetti/Documentazione/7273/10503#collapse. Accessed 4 Mar 2022

Shahroozi Z, Göteman M, Engström J (2022) Fatigue analysis of a point-absorber wave energy converter based on augmented data from a WEC-Sim model calibrated with experimental data. Trends in renewable energies offshore, RENEW 2022 conference. CRC Press, Lisbon, pp 925–933

Sirigu SA, Foglietta L, Giorgi G, Bonfanti M, Cervelli G, Bracco G, Mattiazzo G (2020) Techno-Economic optimisation for a wave energy converter via genetic algorithm. J Mar Sci Eng 8:482. https://doi.org/10.3390/jmse8070482

Sirigu M, Faraggiana E, Ghigo A, Petracca E, Mattiazzo G, Bracco G (2022a) Development of a simplified blade root fatigue analysis for floating offshore wind turbines. Trends in renewable energies offshore, RENEW 2022 conference. CRC Press, Lisbon, pp 935–941

Sirigu M, Faraggiana E, Ghigo A, Bracco G (2022b) Development of MOST, a fast simulation model for optimisation of floating offshore wind turbines in Simscape Multibody. In: WindEurope annual event 2022b, Journal of Physics: Conference Series. Bilbao, p 12003

So R, Casey S, Kanner S, Simmons A, Brekken TKA (2015) PTO-Sim: Development of a power take off modeling tool for ocean wave energy conversion. In: 2015 IEEE power & energy society general meeting. Denver, Colorado, pp 1–5

TLP (2022) Double-acting general purpose cylinders. TLP. https://www.tlpchina.com/?p=864. Accessed 4 Nov 2022

UL Solutions Spain (2014) H2OCEAN. CORDIS EU research results. https://cordis.europa.eu/project/id/288145. Accessed 11 Aug 2023

Wan L, Gao Z, Moan T, Lugni C (2016) Comparative experimental study of the survivability of a combined wind and wave energy converter in two testing facilities. Ocean Eng 111:82–94. https://doi.org/10.1016/j.oceaneng.2015.10.045

Wang Y, Zhang L, Michailides C, Wan L, Shi W (2020) Hydrodynamic response of a combined wind-wave marine energy structure. J Mar Sci Eng 8:253. https://doi.org/10.3390/jmse8040253

Weinsten A, Ho K (2011) WindWaveFloat (WWF): final scientific report. Principle power, Report No. DOE/EE0002651-2. https://www.osti.gov/servlets/purl/1057931. Accessed 17 Aug 2023

WWF France (2023) PHAROS4MPAs. Interreg MED. https://pharos4mpas.interreg-med.eu/. Accessed 11 Aug 2023

Yu Y-H, Tom N, Jenne D (2018) Numerical analysis on hydraulic power take-off for wave energy converter and power smoothing methods. In: ASME 2018 37th international conference on ocean, offshore and Arctic engineering. Madrid

Yunus AC (2010) Fluid mechanics: fundamentals and applications (Si units). Tata McGraw Hill Education Private Limited, New York

Zhang D, Chen Z, Liu X, Sun J, Yu H, Zeng W, Ying Y, Sun Y, Cui L, Yang S, Qian P (2022) A coupled numerical framework for hybrid floating offshore wind turbine and oscillating water column wave energy converters. Energy Convers Manag 267:115933

ZWA Bearings (2023) Cylindrical roller bearing. ZWA. https://zwabearings.com/four-row-cylindrical-roller-bearing-14/. Accessed 5 June 2023